An approach to modeling the chip thickness and cutter workpiece engagement region in 3 and 5 axis ball end milling

Sai Lotfi[a,*], Belguith Rami[a], Baili Maher[b], Dessein Gilles[b], Bouzid Wassila[a]

[a] Unité de Génie de Production Mécanique et Matériaux, ENIS, Route Soukra Km 3, 5-B.P., 1173-3038, Sfax, Tunisia
[b] Université de Toulouse, INPT/ENIT, Laboratoire Génie de Production, 47 Avenue d'Azereix, BP 1629, F-65016, Tarbes Cedex, France

Keywords:
5-axis ball-end milling
Chip thickness
Tool orientation
Engagement region

A B S T R A C T

The determination of the chip thickness in 5-axis ball end milling is most fundamental to calculate the cutting force which affects the machining stability and surface quality. In the 5-axis ball end milling, adding to the parameters of the 3-axis milling we have two important parameters which are the tilt and the lead angles. They affect the engagement region and the chip thickness and modify the cutting forces. Based on the true tooth trajectory and the machining surface geometries, this paper presents a new analytical model of the cutter workpiece engagement (CWE) region and the instantaneous undeformed chip thickness in three and five axis ball end milling. To validate the model a mechanistic force model was used, the simulation was compared to the measured one and a good agreement between them was proved.

1. Introduction

The parts commonly used in mechanical systems, industrial structure and the functional products in the mold, automobile and aerospace industries are complex shapes. These forms are generally obtained by multi-axial milling and specifically by 5-axis milling. In the milling process the cutting forces and process stability, depend on the chip thickness.

In the 3-axis milling, some works have interested to determinate the instantaneous chip thickness. Rao and Rao [1] calculated the chip thickness in the peripheral milling of the vertical planar surface. Dotcheva and Millward [2] presented a method for calculating maximum chip thickness in the corner of the pocket. Sai et al. [3] developed a method for calculating the instantaneous chip thickness in face milling in circular interpolation. These works interest on the influences of the machining parameters as, cutting depth, feed per tooth and cutting speed on the chip thickness. The cinematic of the machine was introduced in the study of Sai and Bouzid [4].

Nishida et al. [5] calculated the uncut chip thickness using a voxel model. The cutting edge and the instantaneous workpiece shape are fully represented by a voxel model. The removal workpiece voxel is calculated along the vector connecting the center of cutting edge with the cutting edge, and then the uncut chip thickness is calculated by analyzing each minute tool rotational angle. The proposed method can calculate the uncut chip thickness beneath the complex surface of the workpiece and specially shaped cutting edge. The method proves height accuracy in the cutting force prediction. Iwabe et al. [6] calculated the chip area of the inclined surface machined by ball end mill cutter by a contour path method using 3D-CAD. The chip area is calculated by the interference of the rake surface and the chip volume. Buj-Corral et al. [7] calculated the (CWE) region based on the geometric tool-workpiece intersection in order to predict topography and surface roughness as a function of cutting parameters. The geometric model is presented in the case of a flat surface machined by a ball end mill on one way strategy. Another phenomenon which influences the (CWE) region and the chip thickness and is not considered in this study is the motion errors of feed drive systems. Nishio et al. [8] investigated the influence of dynamic motion errors of feed drive systems onto the surface machined by a square end mill. The study is extended by Buj-corral et al. [9] In the case of ball-end milling. These previous works present at various and precise modeling of the (CWE) region and instantaneous chip thickness, but they are limited for the milling of the flat surfaces.

In 5-axis ball end milling, two important parameters related to the orientation of the tool are added to the classical 3-axis milling parameters which are the lead and the tilt angle. Some researchers have interested to investigate the influence of these parameters on the 5 axis ball end milling process, particularly the instantaneous chip thickness. In the work of Zheng and Kang [10] the model of the chip thickness considers the lead angle, the tilt angle and the cutter runout. Ozturk et al. [11] presented the effect of the tilt angle and the lead angle on the

* Corresponding author.
E-mail addresses: lotfi_sai@yahoo.com (L. Sai), rami.belguith@gmail.com (R. Belguith), maher.baili@enit.fr (M. Baili), gilles.dessein@enit.fr (G. Dessein), wassilabouzid@yahoo.fr (W. Bouzid).

Nomenclature

S_{hi}	Height of the crest formed by the disc (i)
P_r	Plane perpendicular to the tool axis
P_{ae}	Plane perpendicular to the plane Pr and formed by vectors (ae) and (z)
P_{fz}	Plane perpendicular to the plane Pr and formed by vectors (fz) and (z)
h_c	Instantaneous undeformed chip thickness (mm)
i_0	Tool Helix angle (°)
f_z	feed per tooth per revolution (mm/tooth/rev)
θ	revolution angle (°)
ψ	disc position angle (°)
φ	the positioning angle of the cutting point (°)
R_0	the tool radius (mm)
$R(z)$	the circumference radius of the elementary disc of the tool axis (mm)
e	runout error (mm)
ρ	the initial eccentricity angle (°)
t	the instant time (s)
θ_l	Lead angle (°)
θ_t	Tilt angle (°)
a_e	Radial depth of cut (mm)
a_p	Axial depth of cut (mm)
θst	Start angle in the cutter-workpiece engagement zone (°)
θ_{Ex}	Exit angle in the cutter-workpiece engagement zone (°)
V_f	feed rate (mm/min)
w	spindle speed (rd/s)
n	spindle speed (rev/min)
t	instant time (s)
L	Length of the workpiece (mm)
l	Width of the workpiece (mm)
N_f	number of teeth
db	infinitesimal chip width (mm)
F_t, F_r, F_a	tangential, radial and axial cutting force (N)
kt, kr, ka	tangential, radial and axial cutting force coefficient (N/mm)
F_x, F_y, F_z	cutting force respectively in X, Y and Z direction (N)

5-axis ball end milling process. Using a geometrical approach and CAD software system, they demonstrated that tool posture has an effect on the engagement region, on the scallop height, cutting force and the tool tip contact. Ehsan et al. [12] presented the effect of the orientation of the axis ball end milling on the tool tip contact, the cutting force, torque, deflection and surface quality of the flexible part. The model is analog to the one used on the three axis milling. The tilt angle and the lead angle are interpreted from the position of the CL points. Xin et al. [13] presented a geometrical model of a three-dimensional trochoidal tooth trajectory to determine the instantaneous chip thickness. The model includes the tilt angle, the lead angle and the cutter runout.

A few works of literature have been interested to modulate the chip thickness in the case of 5-axis milling of curved geometries. Sun et al. [14] presented an approach to estimate cutting forces based on the undeformed chip thickness model derived from the relative tool-part motion analysis in the milling of a curved surface. The recent work in this domain was presented by Zerun et al. [15]. A parametric chip thickness model was proposed to distinguish cutter/workpiece engagement area and cutting force considering runout errors. To know at any position of the cutter the instantaneous chip thickness is different to zero, it is important to determinate the borders of the cutter and the workpiece engagement region.

In the previous works, some researchers have been interested in the calculation of the (CWE). In the study of Erdim et al. [16], the (CWE) is calculated from the output cutter location data file by an analytical simulation algorithm. The method determines three boundaries in which the engagement region is delimited: the first and the second are respectively the location of the start angle and the exit angle and the third is the workpiece surface. In the study of Ref. [17], the (CWE) is extracted for each cutter location along the tool path, from the removal volume. Ozturk et al. [18] and Erdim and Sullivan [19] calculated the (CWE) by subtracting it from the swept volume of tool motion. The tool is divided into some elemental disk and the engagement points are extracted using an algorithm, then the start angle and the exit angle are calculated. Sun et al. [20] Calculated the (CWE) using a Z-map model. The workpiece is meshed into small grids whose projection onto the plane is a square. The engaged cutter element can be achieved according to the difference between the cutter element and the projection of the instantaneous workpiece height into the cutter element.

The (CWE) zone between the tool and the machined part represents the integration limits used in the calculation of the cutting force. Cutting thickness can also be modeled correctly by knowing the area of engagement between the part and the tool. The validation of these models requires the modeling of the cutting force. In the mechanistic method, cutting forces are assumed to be proportional to uncut chip thickness or cutter swept volume. Yucesan and Altıntaş [21] proposed a ball-end mill force model based on a mechanistic relationship between cutting force and chip load. This model discretizes the ball-end mill into a series of disks and describes in fairly rigorous detail the ball-end mill geometry and chip thickness calculation. In the study of Ko and Cho [22] the dynamic effect is considered in the chip thickness model. More accuracy in the prediction of the cutting forces is proposed by Altintas and Lee [23] who proposed a mechanistic cutting force model for 3D ball-end milling using instantaneous cutting force coefficients that are independent of the cutting conditions and are set as a function of the instantaneous uncut chip thickness only and considers the size effect produced near the tool tip at the low values of undeformed chip thickness.

The models of the instantaneous chip thickness and the cutter workpiece engagement zone developed above for the calculation of the cutting force consider only the flat surfaces which are perpendicular or inclined relative to the axis of the tool. The new contribution in our study is the geometric modeling in the case of free form surfaces. The models developed in this work calculate the instantaneous undeformed chip thickness, the entrance angle and the exit angle of the (CWE) zone for the surfaces machined in a 3 and 5 axis ball-end milling, then the mechanistic cutting forces are determined.

In this paper, the true cutting edge trajectory is formulated. The parameters considered in the model are the tilt angle, the lead angle, the feed per tooth, the depth of cut, the step over, the cutting speed, the cutter runout and the revolutionary angle. The content is presented in the following section as follows: First, the geometrical description of the trajectory of an arbitrary point P in the (CWE) region is represented in the local coordinate system attached to the center of the tool. Second, these coordinates are transformed to the global coordinate system attached to the workpiece. Third, based on the tooth trajectory and the geometries of the milled surface, the cutter workpiece engagement (CWE) region is analyzed and the entrance and exit angles are calculated. Then, the instantaneous undeformed chip thickness formed between the two successive teeth trajectories had been extracted. A numerical simulation by Matlab software is used to simulate the proposed model. Finally a mechanistic force model is proposed to validate the approach. The predicted forces are compared with the measured ones in the work of Guo et al. [24] and they present a good agreement.

2. General formulation of the coordinate system

In this work, a ball nose end milling cutter with two teeth ($N_f = 2$)

uniformly distributed was considered. P(X_P, Y_P, Z_P) denotes the points of the intersection region between the cutter and the work-piece. The coordinate system is established in order to obtain the parametric equation of the point P on the cutting edge in the global coordinate system R_W attached to the workpiece Fig. 1.

$R_W(O_W, \overrightarrow{X_W}, \overrightarrow{Y_W}, \overrightarrow{Z_W})$: The global coordinate system attached to the workpiece in which the machining surface and the tool path are defined.

$R_H(O_H, \overrightarrow{X_H}, \overrightarrow{Y_H}, \overrightarrow{Z_H})$: The local coordinate system attached to the spindle of the mill machine and moves in the direction of feed rate speed relative to the workpiece.

$R_C(O_C, \overrightarrow{X_C}, \overrightarrow{Y_C}, \overrightarrow{Z_C})$: The local coordinate system fixed on the center of the cutter, considering initially that $\overrightarrow{O_H Y_H}$ and the vector of spindle runout, $\vec{e}$, are aligned. The cutter revolves around the spindle axis $\overrightarrow{O_H Z_H}$. The angle between $\overrightarrow{O_C Y_C}$ and $\overrightarrow{O_H Y_H}$ is $(\theta+\rho)$, with θ is the rotation angle and ρ is the initial eccentricity angle.

$R_N(C_C, \vec{f}, \vec{t}, \vec{n})$: The local coordinate system of any given node C_C (cutter contact point) on the machined surface. $\vec{n}$ is the normal direction of the milled surface, $\vec{f}$ is parallel to the linear feed velocity and $\vec{t}$ is equal to the cross product of $\vec{n}$ and $\vec{f}$.

3. Mathematical description of the cutting edge trajectory

The coordinates of a point P on the i^{th} cutting edge in the local coordinate system $R_C(O_C, \overrightarrow{X_C}, \overrightarrow{Y_C}, \overrightarrow{Z_C})$ as are shown in Fig. 2 are expressed by the Eq. (1) as:

$$\overrightarrow{O_C P}|_{Rc} = \begin{bmatrix} X_P \\ Y_P \\ Z_P \end{bmatrix}_{Rc} = \begin{bmatrix} R(z)cos(\varphi(z)) \\ R(z)sin(\varphi(z)) \\ -R_0\varphi(z)/tan(i_0) \end{bmatrix} \quad (1)$$

The different parameters $\varphi(z)$ and $R(z)$ are calculated as follows:

$$\varphi(z) = \frac{z tan(i_0)}{R_0}$$

$$R(z) = (R_0^2 - (R_0 - z)^2)^{1/2}$$

The position of the point P is written in the coordinate system R_H as:

$$\overrightarrow{O_H P} = \begin{bmatrix} X_P \\ Y_P \\ Z_P \end{bmatrix}_{RH} = \begin{bmatrix} esin(\theta) \\ ecos(\theta) \\ 0 \end{bmatrix}_{R_H} + M_{CH} \begin{bmatrix} X_P \\ Y_P \\ Z_P \end{bmatrix}_{Rc} \quad (2)$$

Where M_{CH} is the matrix transformation from $R_C(O_C, \overrightarrow{X_C}, \overrightarrow{Y_C}, \overrightarrow{Z_C})$ to $R_H(O_H, \overrightarrow{X_H}, \overrightarrow{Y_H}, \overrightarrow{Z_H})$.

$$M_{CH} = \begin{bmatrix} \cos(\theta+\rho) & -\sin(\theta+\rho) & 0 \\ \sin(\theta+\rho) & \cos(\theta+\rho) & 0 \\ 0 & 0 & 1 \end{bmatrix}$$

In order to avoid the tool tip contact on the machined surface, the holder is first rotated by an inclination tilt angle θ_t about the $\vec{f}$ axis vector, then, by a lead angle θ_l about the $\vec{t}$ axis vector, Fig. 3. The transformation matrix M_{NT} from $R_H(O_H, \overrightarrow{X_H}, \overrightarrow{Y_H}, \overrightarrow{Z_H})$ to $R_N(C_C, \vec{f}, \vec{t}, \vec{n})$ is written as:

$$M_{NT} = \begin{bmatrix} \cos(\theta_l) & 0 & \sin(\theta_l) \\ \sin(\theta_t)\sin(\theta_l) & \cos(\theta_t) & -\sin(\theta_t)\cos(\theta_l) \\ -\cos(\theta_t)\sin(\theta_l) & \sin(\theta_t) & \cos(\theta_t)\cos(\theta_l) \end{bmatrix} \quad (3)$$

After the tool orientation, the vector $\overrightarrow{C_C O_H}$ and $\vec{n}$ are aligned Fig. 1, the point C_C is represented in the local coordinate system $R_N(C_C, \vec{f}, \vec{t}, \vec{n})$ by the Eq. (4):

$$\overrightarrow{C_C O_H}|_{R_N} = \begin{bmatrix} 0 \\ 0 \\ R_0 \end{bmatrix}_{R_N} \quad (4)$$

The coordinates of point P in the local coordinate system $R_N(C_C, \vec{f}, \vec{t}, \vec{n})$ are as Eq. (5):

$$\overrightarrow{C_C P} = \begin{bmatrix} X_P \\ Y_P \\ Z_P \end{bmatrix}_{RN} = \begin{bmatrix} 0 \\ 0 \\ R_0 \end{bmatrix}_{R_N} + M_{NT} \begin{bmatrix} esin(\theta) \\ ecos(\theta) \\ 0 \end{bmatrix}_{R_H} + M_{NT} M_{CH} \begin{bmatrix} X_P \\ Y_P \\ Z_P \end{bmatrix}_{Rc} \quad (5)$$

In machining, the obtained surface is represented by the successive cutter contact points C_C between the cutter and the workpiece. There are two cases of machining surfaces.

The first is a closed-form surface which can be formulated by a parametric mathematical equation; it can be a plane or a curved surface. The second is a free-form surface which can be formulated from a cutter contact point extracted from the cutter location data file (CL) obtained from a CAD/CAM software system. In the two cases, we need the matrix transformation from the coordinate system $R_N(C_C, \vec{f}, \vec{t}, \vec{n})$ to the global coordinate $R_W(O_W, \overrightarrow{X_W}, \overrightarrow{Y_W}, \overrightarrow{Z_W})$ attached to the workpiece.

In the first case of closed form, the surface is defined by its parametric form $S(u, v)$, assumed to be different to the first order. In the second case of the free-form surface: the coordinates of point C_C and the three vectors, $\vec{f}$, $\vec{t}$ and $\vec{n}$ are identified by a conversion of the CL points and tool orientation from CNC program using the APT language. For a given point C_C on the surface, the transformation matrix S from the coordinates system $R_N(C_C, \vec{f}, \vec{t}, \vec{n})$ to the global coordinates system $R_W(O_W, \overrightarrow{X_W}, \overrightarrow{Y_W}, \overrightarrow{Z_W})$ is expressed by:

$$M_W = \begin{bmatrix} df_x & df_y & df_z \\ dt_x & dt_y & dt_z \\ dn_x & dn_y & dn_z \end{bmatrix}$$

Where (df_x, df_y, df_z), (dt_x, dt_y, dt_z) and (dn_x, dn_y, dn_z) are respectively the components of the vectors $\vec{f}$, $\vec{t}$ and $\vec{n}$ in the global coordinate R_W. The coordinates of point P in the global coordinate system attached to the workpiece $R_W(O_W, \overrightarrow{X_W}, \overrightarrow{Y_W}, \overrightarrow{Z_W})$ are expressed by Eq. (6):

$$\overrightarrow{O_W P} = \begin{bmatrix} X_P \\ Y_P \\ Z_P \end{bmatrix}_{Rw} = \begin{bmatrix} X_{Cc} \\ Y_{Cc} \\ Z_{Cc} \end{bmatrix} + M_W \begin{bmatrix} 0 \\ 0 \\ R_0 \end{bmatrix}_{R_N} + M_W M_{NT} \begin{bmatrix} esin(\theta) \\ ecos(\theta) \\ 0 \end{bmatrix}_{R_H} + M_W M_{NT} M_{CH} \begin{bmatrix} X_P \\ Y_P \\ Z_P \end{bmatrix}_{Rc} \quad (6)$$

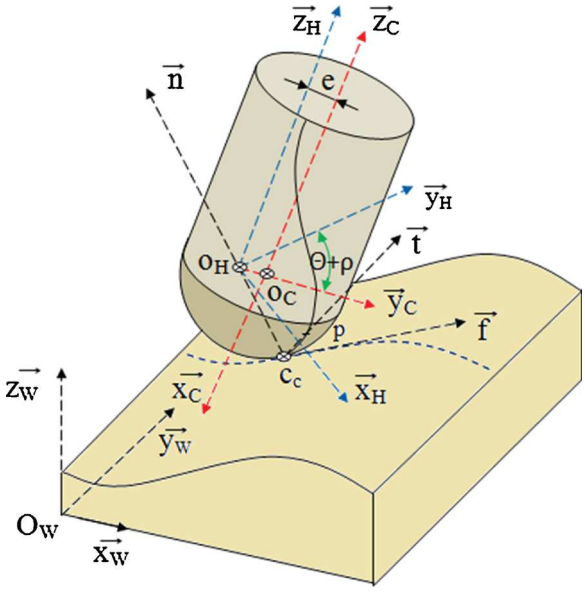

Fig. 1. Configuration of the system coordinates.

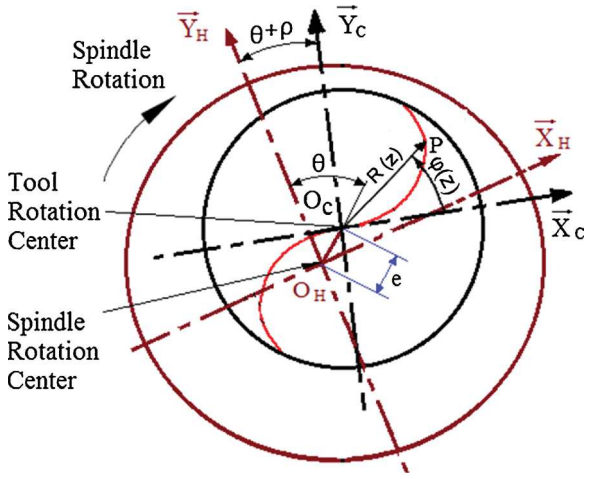

Fig. 2. Location of point P on the cutting edge.

Where: X_{Cc}, Y_{Cc} and Z_{Cc} are the coordinates of point C_C in the global coordinate system R_W.

4. Chip thickness determination

The chip thickness h_C is variable along the cutting edge locally in both tangential and axial directions. In a 3D modeling, instantaneous chip thickness can be calculated through the instantaneous position of the cutter center as depicted in Fig.4. Point N is the instantaneous location on the i^{th} cutting edge at time t_1, the point M denotes the point on the $(i+1)^{th}$ successive cutting edge at time t_2. Point O_{C1} and point O_{C2} represent their corresponding ball centers respectively. Additionally, line $O_{C2}M$ just passes by point N.

The instantaneous chip thickness is determined by the distance MN. Its calculation is based on the mathematical relationship between the tooth paths generated by different teeth on the one milling cutter. The chip thickness for a tooth $(i+1)$ engaged in cutting is determined through finding the intersection point of the path curve left by the preceding tooth (i) and the line passing through the current tooth tip and the cutter axis O_{C2}.

The numerical method to calculate the instantaneous chip thickness consists to determinate the coordinates of points O_{C2}, N and M in the global coordinate system R_W then the vectors $O_{C2}N$ and $O_{C2}M$ are calculated. N and M represent, respectively all the intersection points of the tooth (i) and the workpiece and the tooth $(i+1)$ and the workpiece. When the three points O_{C2}, N and M are aligned the cross vector product is equal to zero. For each points M and N, the Software tests the condition. If the condition is true, it maintains the coordinates of N and M in global coordinate system R_W and calculates the distance MN which is equal to the instantaneous chip thickness h_C. The coordinates of point

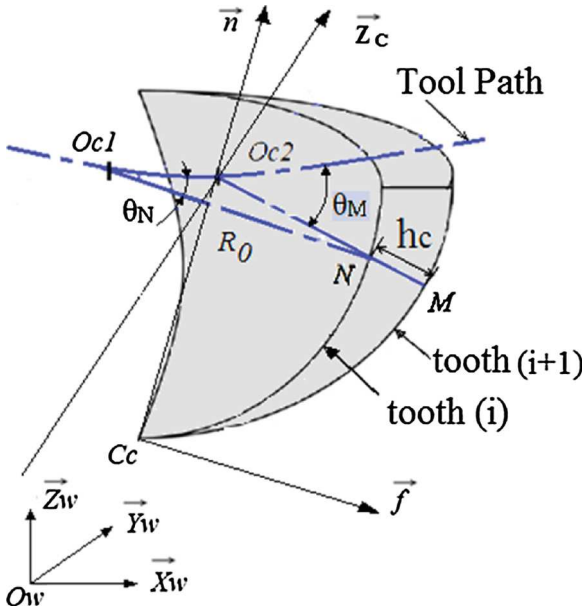

Fig. 4. Chip thickness representation in 5-axis ball-end milling.

N in the global coordinate system R_W at instant t_1 are:

$$\overrightarrow{O_wN} = \begin{bmatrix} X_N \\ Y_N \\ Z_N \end{bmatrix}_{Rw} = \begin{bmatrix} X_{Cc} \\ Y_{Cc} \\ Z_{Cc} \end{bmatrix}(t_1) + M_w(t_1)\begin{bmatrix} 0 \\ 0 \\ R_0 \end{bmatrix}_{R_N} + M_w(t_1)M_{NT}\begin{bmatrix} e\sin(\theta_N) \\ e\cos(\theta_N) \\ 0 \end{bmatrix}_{R_H} + M_w(t_1)M_{NT}M_{CH}(t_1)\begin{bmatrix} X_N \\ Y_N \\ Z_N \end{bmatrix}_{Rc} \quad (7)$$

The coordinates of point O_{C2} center of the cutter in the global coordinate system R_W at instant t_2 are expressed by Eq. (8):

$$\overrightarrow{O_wO_{C2}} = \begin{bmatrix} X_{OC2} \\ Y_{OC2} \\ Z_{OC2} \end{bmatrix}_{Rw} = \begin{bmatrix} X_{Cc} \\ Y_{Cc} \\ Z_{Cc} \end{bmatrix}(t_2) + M_w(t_2)\begin{bmatrix} 0 \\ 0 \\ R_0 \end{bmatrix}_{R_N} + M_w(t_2)M_{NT}\begin{bmatrix} e\sin(\theta_M) \\ e\cos(\theta_M) \\ 0 \end{bmatrix}_{R_H} \quad (8)$$

The coordinates of point M in the global coordinate R_W at instant t_2 are expressed by Eq. (9):

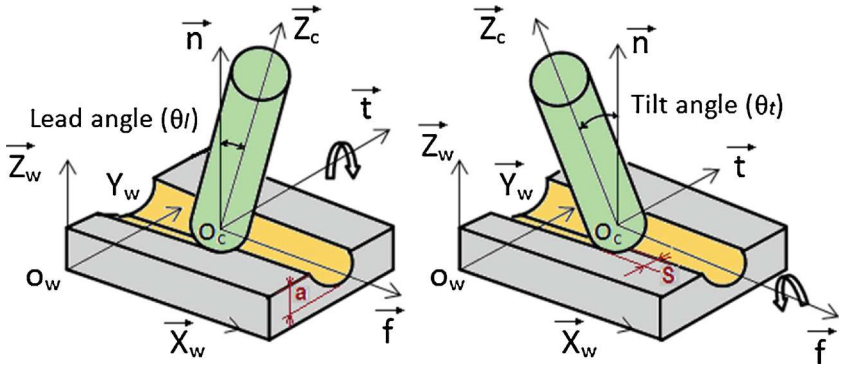

Fig. 3. Tool orientations in 5-axis milling.

$$\overrightarrow{O_wM} = \begin{bmatrix} X_M \\ Y_M \\ Z_M \end{bmatrix}_{Rw} = \begin{bmatrix} X_{Cc} \\ Y_{Cc} \\ Z_{Cc} \end{bmatrix}(t_2) + M_w(t_2)\begin{bmatrix} 0 \\ 0 \\ R_0 \end{bmatrix}_{RN} + M_w(t_2)M_{NT}\begin{bmatrix} e\sin(\theta_M) \\ e\cos(\theta_M) \\ 0 \end{bmatrix}_{RH} + M_w(t_2)M_{NT}M_{CH}(t_2)\begin{bmatrix} X_M \\ Y_M \\ Z_M \end{bmatrix}_{Rc} \quad (9)$$

The points O_{C2}, N and M are located on the same line. The coordinates of points M and N confirm the Eq. (10) with "× "denotes the cross section product.

$$\overrightarrow{Oc_2N} \times \overrightarrow{Oc_2M} = \vec{0} \quad (10)$$

The vector $\overrightarrow{O_{C2}M}$ is expressed by the Eq. (11) as:

$$\overrightarrow{O_{C2}M} = M_W(t_2)M_{NT}M_{CH}(t_2)\begin{bmatrix} X_M \\ Y_M \\ Z_M \end{bmatrix}_{Rc} \quad (11)$$

The vector $\overrightarrow{O_{C2}N}$ is expressed by the Eq. (12) as:

$$\overrightarrow{O_{C2}N} = \begin{bmatrix} X_{Cc} \\ Y_{Cc} \\ Z_{Cc} \end{bmatrix}(t_1) - \begin{bmatrix} X_{Cc} \\ Y_{Cc} \\ Z_{Cc} \end{bmatrix}(t_2) + [M_w(t_1) - M_w(t_2)]\begin{bmatrix} 0 \\ 0 \\ R_0 \end{bmatrix}_{RN} + M_w(t_1)M_{NT}\begin{bmatrix} e\sin(\theta_N) \\ e\cos(\theta_N) \\ 0 \end{bmatrix}_{RH} - M_w(t_2)M_{NT}\begin{bmatrix} e\sin(\theta_M) \\ e\cos(\theta_M) \\ 0 \end{bmatrix}_{RH} + M_w(t_1)M_{NT}M_{CH}(t_1)\begin{bmatrix} X_N \\ Y_N \\ Z_N \end{bmatrix}_{Rc} \quad (12)$$

When the two vectors $\overrightarrow{O_{C2}M}$ and $\overrightarrow{O_{C2}N}$ are known the instantaneous undeformed chip thickness h_c is calculated by:

$$h_C(\theta, z) = \overrightarrow{O_{C2}M} - \overrightarrow{O_{C2}N} \quad (13)$$

Noting that, θ_{St} and θ_{Ex} are respectively, the start angle and the exit angle in the (CWE) zone. The instantaneous undeformed chip thickness $h_c(\theta, z)$ is expressed by Eq. (14).

$$h(\theta, z) = \begin{cases} h_c(\theta, z) & \theta_{St} \le \theta \le \theta_{Ex},\ 0 \le z \le ap \\ 0 & else \end{cases} \quad (14)$$

In the next section we interest to modeling the (CWE) region.

5. (CWE) for 3-axis ball end milling

The (CWE) determination is not easy in ball end milling. The engagement region for any elementary disc is bounded between the start angle and the exit angle. Fig. 5 shows the representation of the different (CWE) zones and the planes utilized for a 2D view. Fig. 6 shows the two successive cutter positions. The first is in the cross feed direction, view in the plane (Pa_e) and the second is in the feed direction, view in the plane (Pf_z). In the ball end milling process, the tooth feed f_z is kept to comparably less than the radial depth of cut a_e. In general the ratio feed/radial depth (f_z /a_e) is less than one third. For these reasons, the (CWE) is divided into three zones. The zone-I is the region for $2R(z) > a_e$ and the zone-II is the region for $2R(z) < a_e$ as is shown in the view in the plane (Pa_e) as shown in Fig. 6. The zone-II is so divided on two zones. Zone-II-1 is the region for $f_z < 2R(z) < a_e$ and the zone-II-1 is the region for $2R(z) < f_z$ as is shown in the view in the plane (Pf_z).

5.1. The Engagement Zone-I

In the plane view (Pr), the distance between the initial and final workpiece curves is the radial depth of cut a_e. This region represents the material removed for one pass. The zone-I is the region, which the point P in the cutting edge exits on the initial workpiece curve as is shown in Fig.7. The produced chip is represented by the ABC area. The curves AB and AC are two successive teeth trajectories, points B and C are respectively exit points of the teeth (i) and ($i+1$) at a distance of instantaneous feed per tooth f_z.

The entry and exit angles corresponding to $(i+1)^{th}$ tooth trajectory are expressed as follows:

$$\theta_{St}(z) = -\cos^{-1}(1-S_{h1}(z)/R(z)) + \varphi(z)\theta_{EX}(z) = \cos^{-1}((R_0 - ae)/R(z)) + \varphi(z) \quad (15)$$

The calculation of the start angle needs the determination of the distance $S_{h1}(z)$.

Thereafter we develop the method to determinate the distance $S_{hi}(z)$ for any arbitrary disc with radius $R(z)$. In the view on plane Pr, the tooth trajectory is trochoidal. The approximation of the trochoidal arc that generates the profiles to a circular arc as is shown in Fig. 8 is not

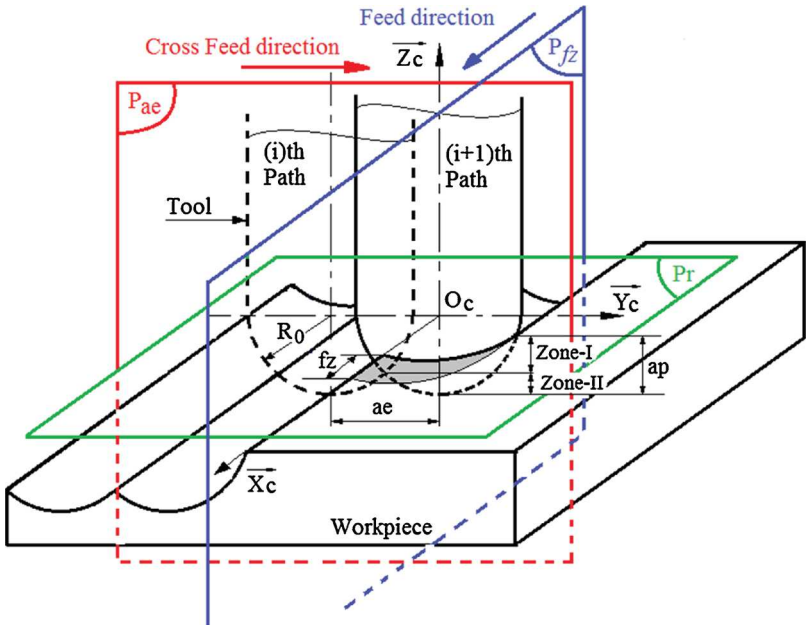

Fig. 5. CWE region representation in 3D view.

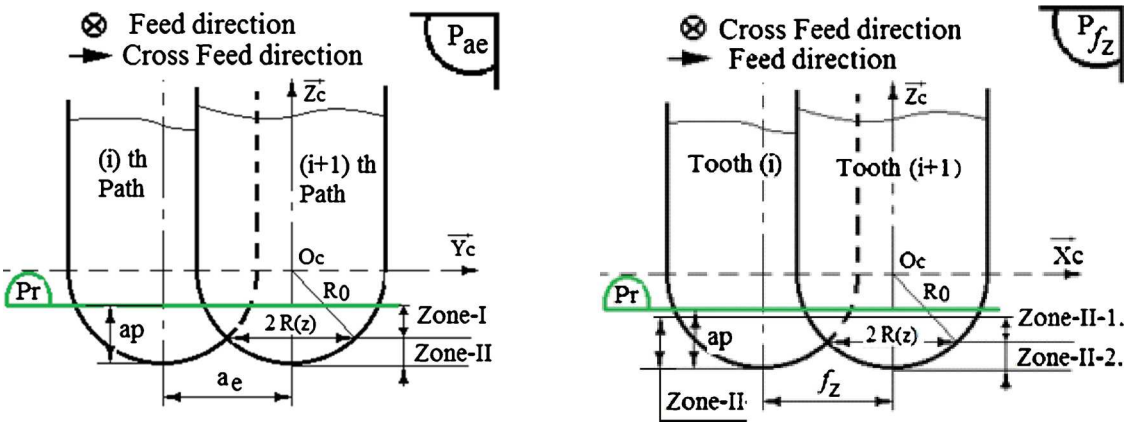

Fig. 6. Different view of the (CWE) region in ball end milling.

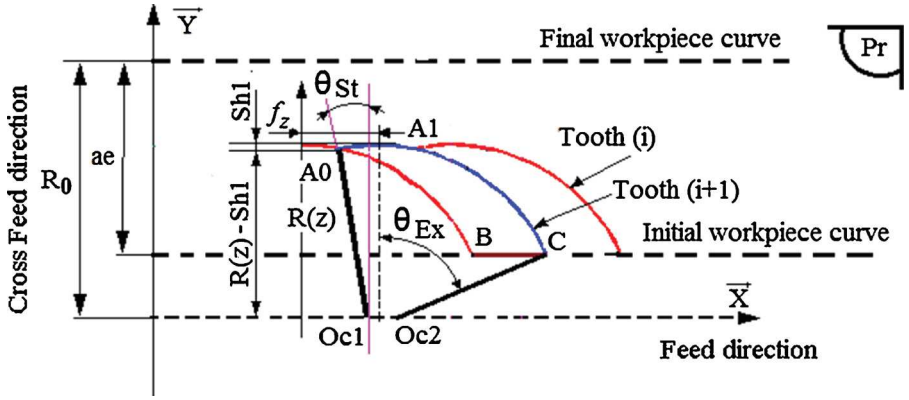

Fig. 7. Teeth trajectory, start and exit angles in the Zone-I.

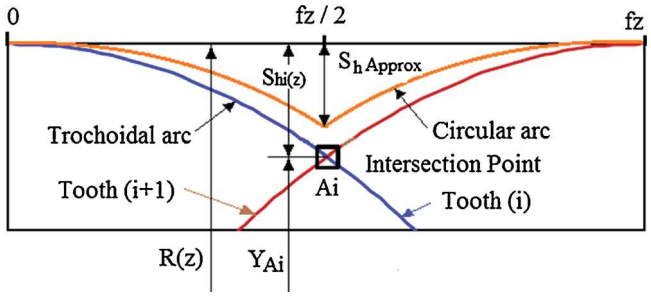

Fig. 8. Approximation of trochoidal arcs to circular arcs.

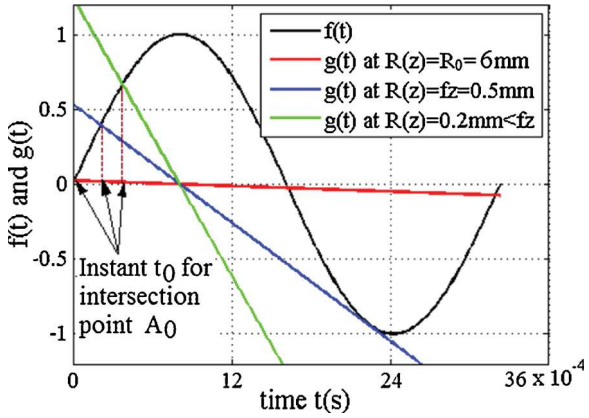

Fig. 9. Instant time of start position of tooth (i), $X(t)=f_z/2$, $R_0 = 6$ mm, $f_z = 0.5$ mm/tooth, $n = 1500$ rev/min.

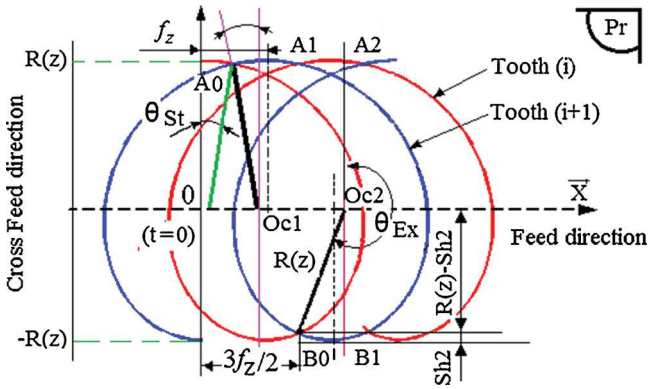

Fig. 10. Start and exit angle of the engagement region (Zone –II-1).

correct. For determining the exact distance $S_{hi}(z)$, the coordinates of the point A_i in the cutter workpiece engagement region must be known first. The start point A_i at θ_{St} start angle of the (i^{th}) rotation of the (i^{th}) tooth verifies the equations of the trajectory Eq. (16):

$$X_{Ai}(t_i) = V_f t_i + e\sin(wt_i) + R(z)\sin(wt_i + \rho - \varphi(z)) = (2k+1)f_z/2 \quad (16\text{-}1)$$

$$Y_{Ai}(t_i) = e\cos(wt_i) + R(z)\cos(wt_i + \rho - \varphi(z)) \quad (16\text{-}2)$$

Where V_f is the feed rate, t_i is the instant time, k is an integer, the distance $S_{hi}(z)$ at point A_i is expressed by:

$$S_{hi}(z) = R(z) - Y_{Ai}(t_i) = R(z)(1 - \cos(wt_i + \rho - \varphi(z))) - e\cos(wt_i) \quad (17)$$

For the elementary discretized disc with an effective radius $R(z)$, the

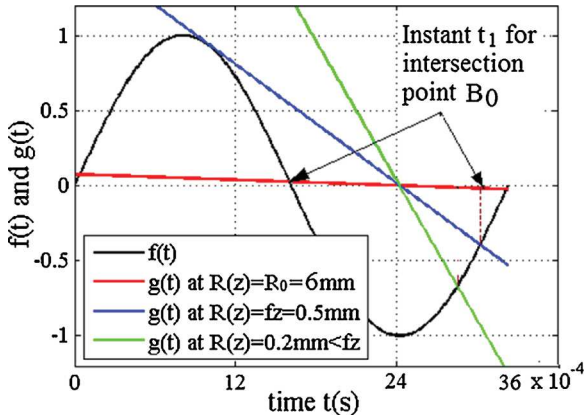

Fig. 11. Instant time of Exit position of tooth (i), $X(t)=3f_z/2$, $R_0=6$mm, $f_z=0.5$mm/tooth, $n=1500$ rev/min, $e=0$mm and $\rho=0^\circ$.

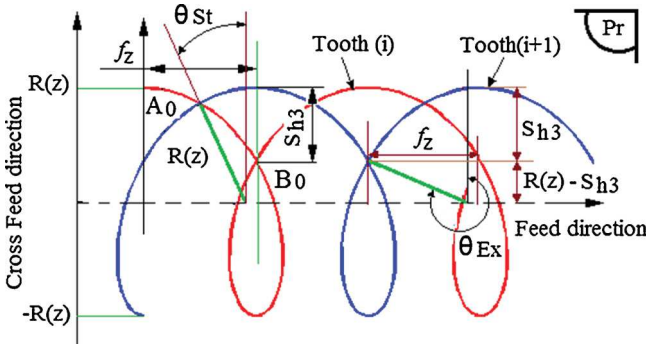

Fig. 12. Start and exit angle (Zone –II-2).

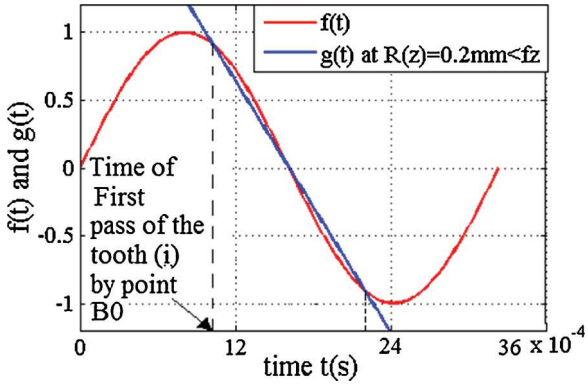

Fig. 13. Instant time of start position of tooth (i), $X(t)=f_z/2$, $R_0=6$ mm, $f_z=0.5$ mm/tooth, $n=1500$ rev/min, $e=0$ mm and $\rho=0^\circ$.

only unknown in this equation is the instant time t_i which must be determined through the Eq. (16-1) which can be written as:

$$esin(wt_i)/R(z) + \sin(wt_i + \rho - \varphi(z)) = \frac{(2k+1)f_z}{2R(z)} - \frac{V_f}{R(z)}t_i \tag{18}$$

Considering the two functions as follows:

$$f(t) = esin(wt)/R(z) + \sin(wt + \rho - \varphi(z))$$

$$g(t) = \frac{(2k+1)f_z}{2R(z)} - \frac{V_f}{R(z)}t \tag{19}$$

A graphical resolution for one rotation of the tool is shown in Fig. 9. For $k=0$ the instant t_0 is the instant when the tooth (i) is at A_0. For the first pass of the tooth (i) by the point A_0, the traveled distance is equal to $f_z/2$ correspond to the first intersection between the two functions f

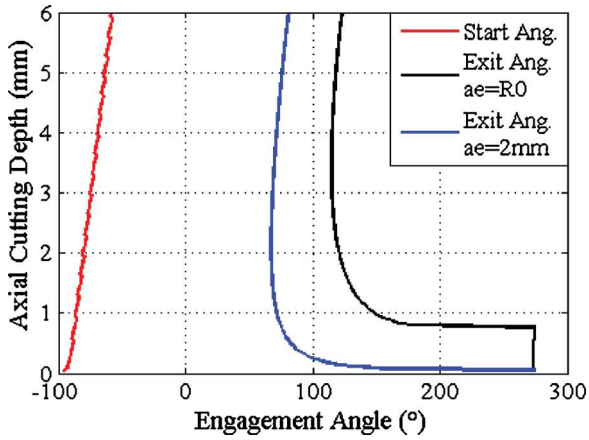

Fig. 14. Start and exit angles along the cutter axis in 3-axis ball end milling. $R_0=6$ mm, $f_z=0.2$ mm/tooth/rev, $a_p=6$ mm, $n=1500$ rev/min, $e=0$ mm and $\rho=0^\circ$.

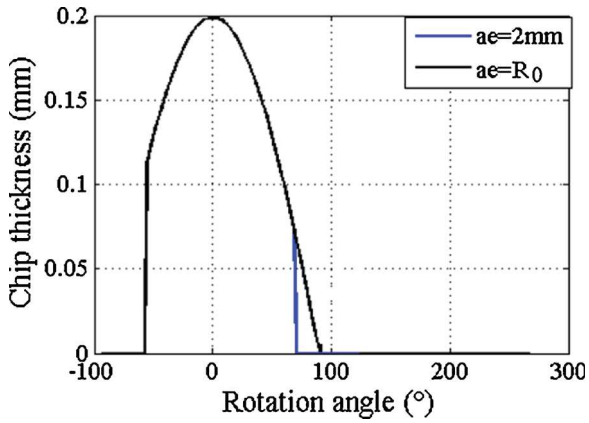

Fig. 15. Chip thickness as a rotation angle in 3-axis ball end milling. $R_0=6$ mm, $f_z=0.2$ mm/tooth/rev, $a_p=6$ mm, $n=1500$ rev/min, $e=0$ mm and $\rho=0^\circ$.

(t) and $g(t)$. The tooth trajectory passes with the coordinate $X(t)=f_z/2$ three times for $R(z)=R_0$, two times for $R(z)=f_z$ and one time for $R(z)<f_z$ as is shown in Fig. 9. The first points of intersection of the two function $f(t)$ and $g(t)$ are at the instant t_0 for the intersection point A_0. When the time t_0 is known the distance S_{h1} is known and the start angle and the exit angle are calculated from Eq. (15).

5.2. The Zone-II-1

The trajectory of point P in the engagement Zone-II-1 is shown in Fig. 10. This zone is characterized by the condition ($f_z \le 2R(z) \le a_e$). The start angle is calculated as in the zone-I. The exit angle is calculated when the tooth (i) is reached at the position of point B_0. The instant t_1 is calculated by the resolution of the Eq. (19) for $k=1$. The traveled distance by the tooth (i) from zero to exit point B_0 in X direction is $X(t)=3f_z/2$. The tooth passes three times by the X coordinates equal to $3f_z/2$. The point B_0 corresponds to the second passage. In the graphical resolution the time t_1 corresponds to the second intersection of the two functions $f(t)$ and $g(t)$ as is shown in Fig. 11. When the time t_1 is known, the distance S_{h2} is calculated and the exit angle is calculated. The start angle and the exit angle are expressed by the Eq. (20):

$$\theta_{St}(z) = -\cos^{-1}(1-S_{h1}(z)/R(z)) + \varphi(z),\ \theta_{EX}(z) = \pi + \cos^{-1}(1-S_{h2}(z)/R(z)) + \varphi(z) \tag{20}$$

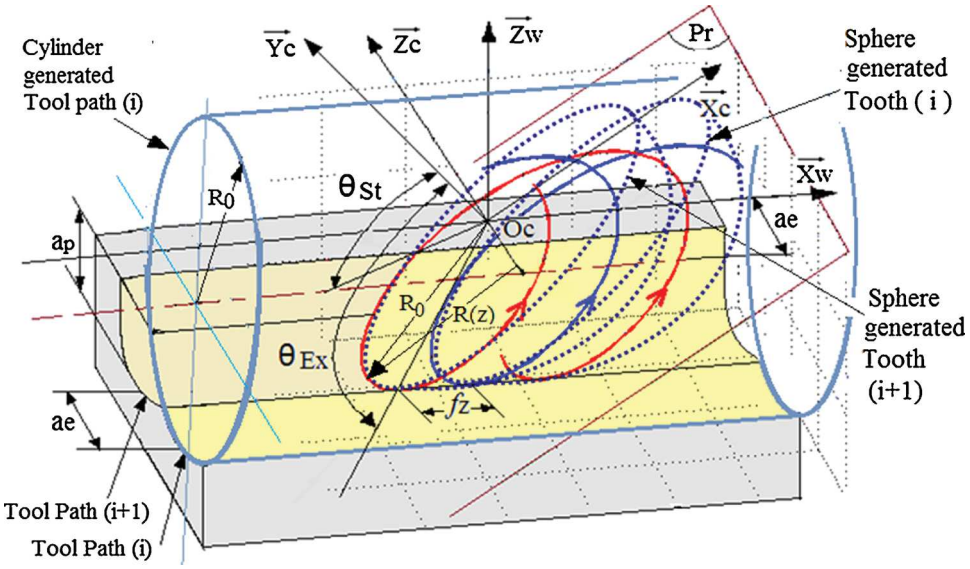

Fig. 16. Start and Exit point in the case of the five-axis ball end milling.

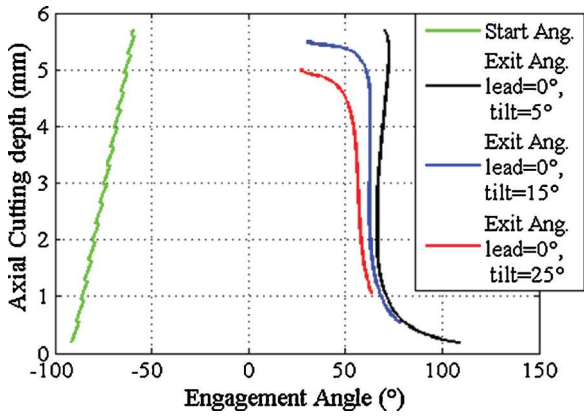

Fig. 17. (CWE) region along the cutter axis for orientation tool angles, $\theta_t = 5^{\circ}$, $\theta_t = 15^{\circ}$ and $\theta_t = 25^{\circ}$, for $R_0 = 6$ mm, $f_z = 0.2$ mm/tooth/rev, $a_e = 2$ mm, $a_p = 5$ mm, $n = 1500$ rev/min, $e = 0$ mm and $\rho = 0^{\circ}$.

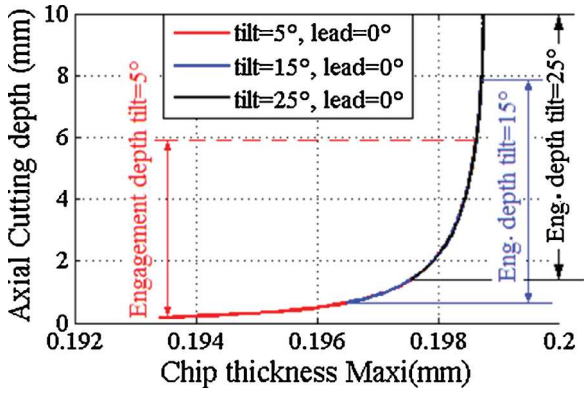

Fig. 18. Maximum chip thickness along the cutter axis for orientation tool angles, $\theta_t = 5^{\circ}$, $\theta_t = 15^{\circ}$ and $\theta_t = 25^{\circ}$, for $R_0 = 6$ mm, $f_z = 0.2$ mm/tooth/rev, $a_e = 2$ mm, $a_p = 5$ mm, $n = 1500$ rev/min, $e = 0$ mm and $\rho = 0^{\circ}$.

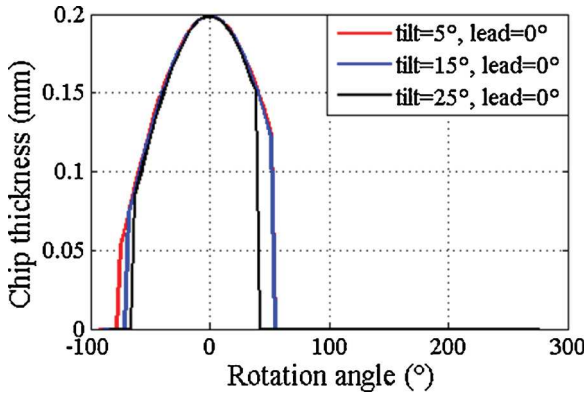

Fig. 19. Chip thickness as cutter revolution for orientation tool angles, $\theta_t = 5^{\circ}$, $\theta_t = 15^{\circ}$ and $\theta_t = 25^{\circ}$, for $R_0 = 6$ mm, $f_z = 0.2$ mm/tooth/rev, $a_e = 2$ mm, $a_p = 5$ mm, $n = 1500$ rev/min, $e = 0$ mm and $\rho = 0^{\circ}$.

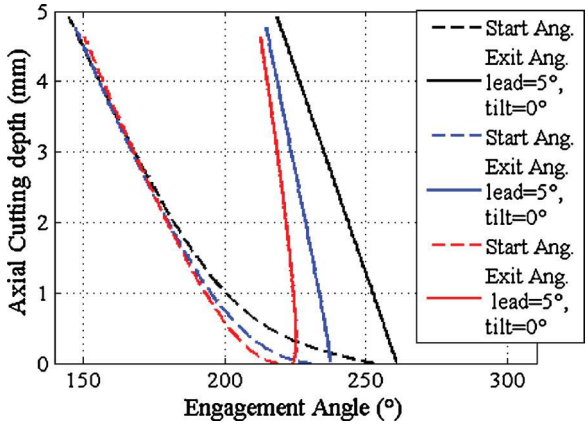

Fig. 20. (CWE) region along the cutter axis for orientation tool angles, $\theta_l = 5^{\circ}$, $\theta_l = 15^{\circ}$ and $\theta_l = 25^{\circ}$, for $R_0 = 6$ mm, $f_z = 0.2$ mm/tooth/rev, $a_e = 2$ mm, $a_p = 5$ mm, $n = 1500$ rev/min, $e = 0$ mm and $\rho = 0^{\circ}$.

5.3. The Zone-II-2

The point P on the (CWE) region Zone-II-2 rotates and does not intersect in the previous cutting tooth trajectory at the exit point as is shown in Fig. 12. The zone II-2 is characterized by the condition $(0 \le 2R(z) \le f_z)$. The start angle is calculated for instant time t_0 when the tooth travels a distance $X(t) = f_z/2$ at point A_0 as was developed previously. The exit angle is calculated for the instant t_1 at point B_0 when the tooth travels a distance equal to f_z. The instant t_1 is the graphical solution of the Eq. (19) for the first pass of the tooth (i) from

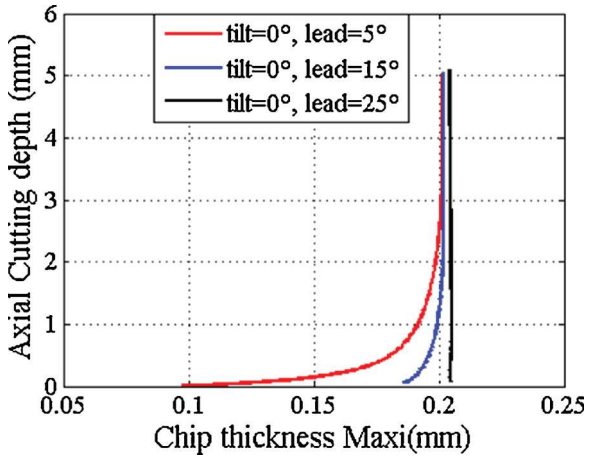

Fig. 21. Maximum chip thickness along cutter axis for orientation tool angles, $\theta_l = 5^\circ$, $\theta_l = 15^\circ$ and $\theta_l = 25^\circ$, for $R_0 = 6$ mm, $f_z = 0.2$ mm/tooth/rev, $a_e = 2$ mm, $a_p = 5$ mm, $n = 1500$ rev/min, $e = 0$ mm and $\rho = 0^\circ$.

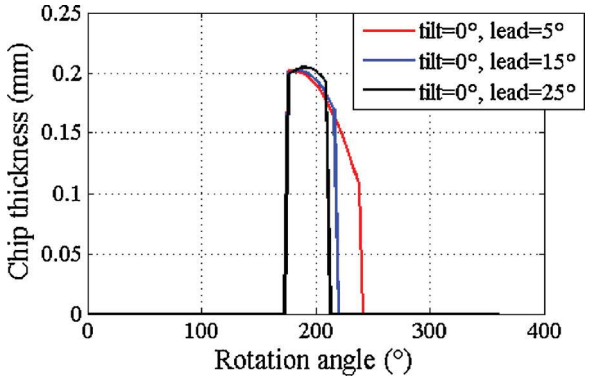

Fig. 22. Chip thickness as a cutter revolution for orientation tool angles, $\theta_l = 5^\circ$, $\theta_l = 15^\circ$ and $\theta_l = 25^\circ$, for $R_0 = 6$ mm, $f_z = 0.2$ mm/tooth/rev, $a_e = 2$ mm, $a_p = 5$ mm, $n = 1500$ rev/min, $e = 0$ mm and $\rho = 0^\circ$.

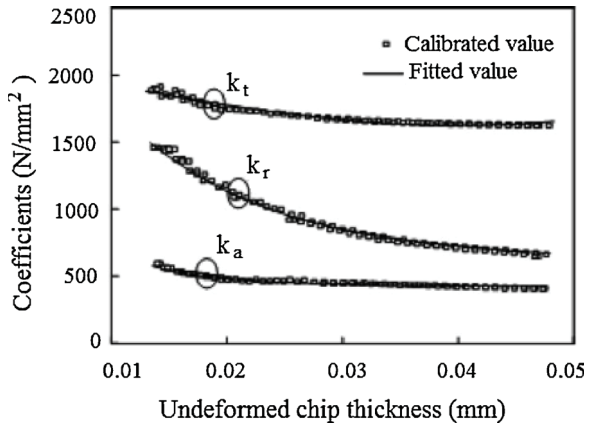

Fig. 23. Calibrated cutting coefficients, Guo et al. [24].

point B_0 Fig. 13. When the instant t_1 and the distance S_{h3} are known, the exit angle can be calculated. The start angle and the exit angle are respectively expressed as follows:

$$\theta_{St}(z) = -\cos^{-1}\left(1 - \frac{S_{h1}(z)}{R(z)}\right) + \varphi(z),\ \theta_{EX}(z) = 2\pi - \cos^{-1}(1 - S_{h3}(z)/R(z)) + \varphi(z) \quad (21)$$

In the ball end milling process, the (CWE) region varies along the cutter axis. The engagement region is calculated between the lower and the higher elementary discs in contact on the workpiece and for each discrete disc between the start and exit angle.

The Fig. 14 shows the variation of the start angle and the exit angle. For the same immersion depth, the engagement region is more important when the radial depth increases and in the same radial depth of cut, the engagement region decreases when the immersion depth increases. The instantaneous chip thickness as a function of the rotation angle is represented by the Fig. 15. It is shown that the maximum is not influenced by the dimension of the (CWE) region.

6. (CWE) in 5-axis ball end milling

The trochoidal tooth trajectory after tool orientation is not planar. So the previous analytical model of the (CWE) region developed in the previous section is not applicable. For this reason a new approach is proposed to determinate the start angle and the exit angle. This approach consists to considerate that $(i)^{th}$ tooth trace on the workpiece is a sphere and the form generated by the $(i)^{th}$ tool path is a cylinder as is shown in Fig.16.

The $(i)^{th}$ tool path generates a cylinder with radius R_0 and axis ($(0, -ae, 0)$, $\overrightarrow{Xw}$). Its equation is:

$$(Y_W - a_e)^2 + Z_w^2 = R_0^2,\ 0 \le X_w \le L \quad (22)$$

At instant t_1 the tooth generates a sphere centered in O_{c1} and with a radius R_0. Its equation is:

$$Y_w^2 + Z_w^2 + (X_w - X_{Oc1})^2 = R_0^2 \quad (23)$$

The coordinates of start point (X_{Pst}, Y_{Pst}, Z_{Pst}) located at start angle θ_{st} are determined by the intersection of the tooth trajectory at t_2 expressed by Eq. (24) and the spherical form expressed by Eq. (25).

$$\begin{bmatrix} X_{PSt} \\ Y_{PSt} \\ Z_{PSt} \end{bmatrix}_{RW} = \begin{bmatrix} X_{Cc} \\ Y_{Cc} \\ Z_{Cc} \end{bmatrix} + M_W(t_2) \begin{bmatrix} 0 \\ 0 \\ R_0 \end{bmatrix}_{RN} + M_W(t_2) M_{NT} \begin{bmatrix} e\sin(\theta_{St}) \\ e\cos(\theta_{St}) \\ 0 \end{bmatrix}_{RH} + M_W(t_2) M_{NT} M_{CH}(t_2) \begin{bmatrix} X_P \\ Y_P \\ Z_P \end{bmatrix}_{Rc} \quad (24)$$

$$(X_{P_{St}} - X_{Oc1})^2 + (Y_{P_{St}} - a_e)^2 + Z_{P_{St}}^2 = R_0^2 \quad (25)$$

The coordinates of the exit point (X_{PEx}, Y_{PEx}, Z_{PEx}) are the solution of the intersection of the trajectory of the tooth $(i+1)$ at instant t_2 expressed by Eq. (26) and the cylinder generated by the previous tool path expressed by Eq. (27):

$$\begin{bmatrix} X_{P_{Ex}} \\ Y_{P_{Ex}} \\ Z_{P_{Ex}} \end{bmatrix}_{RW} = \begin{bmatrix} X_{Cc} \\ Y_{Cc} \\ Z_{Cc} \end{bmatrix} + M_W(t_2) \begin{bmatrix} 0 \\ 0 \\ R_0 \end{bmatrix}_{RN} + M_W(t_2) M_{NT} \begin{bmatrix} \mathrm{esin}(\theta_{Ex}) \\ e\cos(\theta_{Ex}) \\ 0 \end{bmatrix}_{RH} + M_W(t_2) M_{NT} M_{CH}(t_2)(t_2) \begin{bmatrix} X_P \\ Y_P \\ Z_P \end{bmatrix}_{Rc} \quad (26)$$

$$(Y_{P_{Ex}} - a_e)^2 + Z_{P_{Ex}}^2 = R_0^2,\ 0 \le X_{P_{Ex}} \le L \quad (27)$$

The Fig. 17 shows the variation of the (CWE) region for three tool orientations ($\theta_l = 0^\circ$, $\theta_t = 0^\circ$), ($\theta_l = 0^\circ$, $\theta_t = 15^\circ$) and ($\theta_l = 0^\circ$, $\theta_t = 25^\circ$). It can be seen that the cutting edge length increases when the tilt angle increases. So for the same axial cutting depth, the (CWE) region is not more influenced by the tilting orientation. The maximum chip thickness calculated for each (CWE) region is not influenced by the tilt orientation as is shown in Fig.18 and the maximum is reached at the same rotation angle for the three tool orientations as is shown in Fig. 19.

The Fig. 20 shows the important influence of the lead angle orientation on the (CWE) region it is larger when the lead angle increases. So for the same cutting depth, the chip thickness increases when the lead angle increases as is shown in Fig. 21. For the same cutting depth, the maximum value of the instantaneous chip thickness is not changed

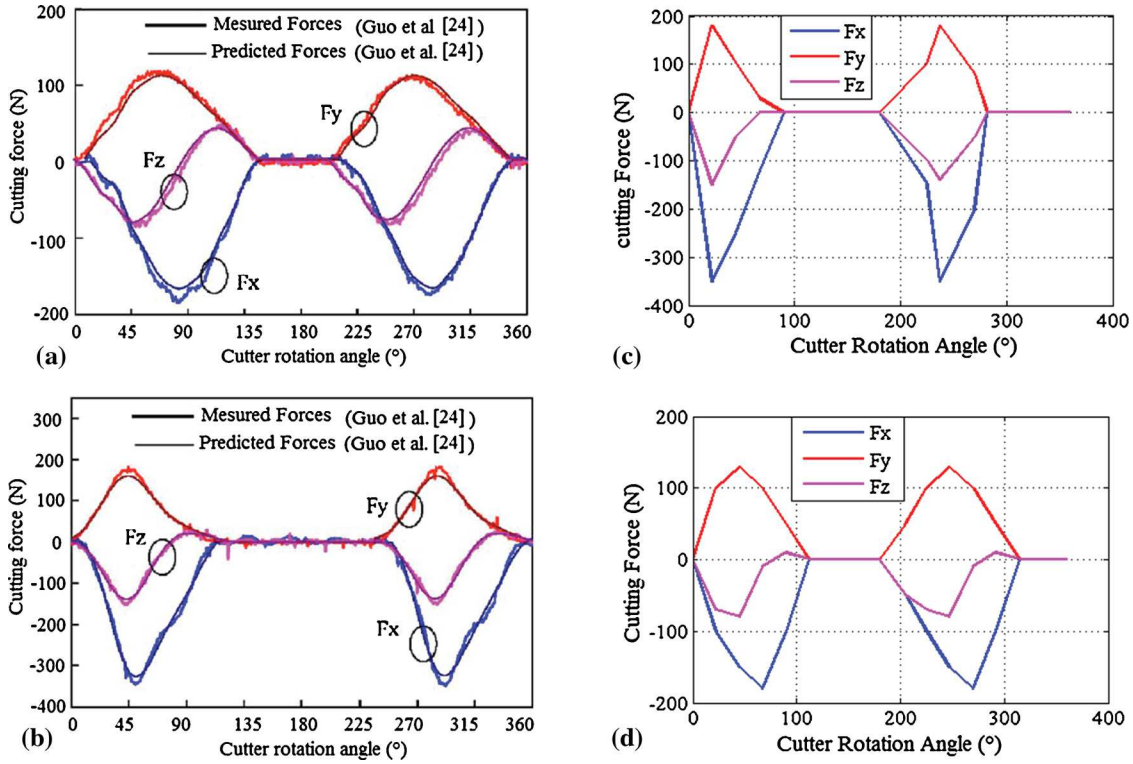

Fig. 24. Comparison of the simulated forces to the measured ones by Guo et al. [24].
(a-c): $\theta_l = 30^\circ$, $\theta_t = 20^\circ$, $a_p = 0.8$ mm,$f_z = 0.1$ mm/tooth/rev, $n = 500$ rpm.
(b-d): $\theta_l = 15^\circ$, $\theta_t = 0^\circ$, $a_p = 1.4$ mm, $f_z = 0.2$ mm/tooth/rev, $n = 1500$ rpm.

when changing the tool orientation by a lead angle but its location changes as is shown in Fig. 22.

7. Experimental validation according to cutting force evolution

In mechanistic model, the cutting force is assumed to be proportional to the undeformed chip thickness. The model adopted in this work is presented by Guo et al. [24] and is expressed by the Eq. (28).

$$\begin{aligned} dF_t(\theta, z) &= k_t(t_n).\, t_n(\theta, z) db(z) \\ dF_r(\theta, z) &= k_r(t_n).\, t_n(\theta, z) db(z) \\ dF_a(\theta, z) &= k_a(t_n).\, t_n(\theta, z) db(z) \end{aligned} \tag{25}$$

Where dF_t, dF_r and dF_a are the differentials cutting forces, respectively, the tangential, the radial and the axial at an arbitrary cutter rotation angle θ and axial differential tool element disc z. k_t, k_r, k_a are respectively the tangential radial and axial cutting force coefficients (N/mm^2). The chip width $db(z)$ is expressed by:

$$db(z) = dz/\sin(\kappa) \tag{29}$$

Cutting force coefficients are determined by a mechanistic calibration procedure and are presented in Fig. 23. The matrix that transforms the cutting forces into the workpiece coordinate $R_W(O_W, \overrightarrow{X_W}, \overrightarrow{Y_W}, \overrightarrow{Z_W})$ is expressed by:

$$A = \begin{bmatrix} -\cos(\theta) & -\sin(\kappa)\sin(\theta) & -\cos(\kappa)\sin(\theta) \\ \sin(\theta) & -\sin(\kappa)\cos(\theta) & -\cos(\kappa)\cos(\theta) \\ 0 & \cos(\kappa) & -\sin(\kappa) \end{bmatrix} \tag{30}$$

The cutting force in the workpiece coordinate which is also a dynamometer coordinate is:

$$\begin{bmatrix} F_x \\ F_y \\ F_z \end{bmatrix}_{Rw} = M_{NT} A \sum_{n=1}^{Nf} \sum_{k=1}^{K} \begin{bmatrix} dF_t \\ dF_r \\ dF_a \end{bmatrix}_{Rc} \tag{31}$$

Two cutting tests are chosen from the work of Guo et al. [24] to validate the model. The material milled is the aluminum 7075-T6. The cutter is a ball end mill with two flutes, 12 mm diameter and 30° helix angle in the vertical CNC milling machine. The cutting forces are measured by a three components dynamometer YDX-III97. The cutting conditions for the two tests are listed in the caption of the Fig. 24.

The cutting forces are predicted for one revolution. The Fig. 24c shows the simulated cutting forces when the tool is orientated by a tilt angle $\theta_t = 20^\circ$ and a lead angle $\theta_l = 30^\circ$ the measured ones in this case are represented by the Fig. 24a. In the second case the simulated forces when the tool is orientated by a tilt angle $\theta_t = 0^\circ$ and a lead angle $\theta_l = 15^\circ$ are presented by the Fig. 24d. The related measured ones are shown by the Fig. 24b.

Good agreements between the predicted and the measured forces are illustrated in both shape and magnitude. The prediction errors defining as the deference between the absolute maximum value of measurement and prediction in percentage not exceed 6%. The obtained results prove the validity of the proposed approach of the (CWE) region and the instantaneous undeformed chip thickness.

8. Conclusions and future works

In this paper, an analytical approach is used to investigate the instantaneous chip thickness in 5-axis ball-end milling. Based on the 3D tooth trajectories (CWE) region had been determined. After that, the instantaneous undeformed chip thickness was determined and its maximum was analyzed. It can be concluded that the tool posture has no effect on the value of the maximum undeformed chip thickness but it has an effect on its location. The (CWE) region is more influence by the tool orientation, it increases when the tool inclination angle increases and causes an elevation of the cutting force magnitude. The cutting force was calculated and was simulated for various tool postures. A comparison of the proposed method and experiments are reported. It shows that the prediction has a good agreement with the experimental

results. We propose as perspectives in the future work to consider the flexion of the tool, to consider the cutting forces for a simulation of the zone of stability.

Acknowledgment

The work is carried out thanks to the support and funding allocated to the Unit of Mechanical and Materials Production Engineering (UGPM2 / UR17ES43) by the Tunisian Ministry of Higher Education and Scientific Research.

References

[1] Rao VS, Rao PVM. Modeling of tooth trajectory and process geometry in peripheral milling of curved surface. Int J Mach Tools Manuf 2005;45:617–30.
[2] Dotcheva M, Millward H. The application of tolerance analysis to the theoretical and experimental evaluation of a CNC Corner milling. Mater Process Tech 2005;170:284–97.
[3] Sai L, Bouzid W, Zghal A. Chip thickness analysis for different tool motions for adaptive feed rate. Mater Process Tech 2008;204:213–20.
[4] Sai L, Bouzid W. Influence of velocity profile on the chip thickness and material removal rate in milling. Int J Mach Mach Mater 2014;16(1):65–79.
[5] Nishida I, Okumura R, Sato R, Shirase K. Cutting force prediction of ball end milling based on fully voxel representation of cutting edge and instantaneous workpiece shape. ASME J Manuf Sci Eng 2018;140(2):1–5.
[6] Iwabe H, Shimizu K, Sasaki M. Analysis of cutting mechanism by ball end mill using 3D-CAD. JSME Int J Ser C 2006;49(1):28–34.
[7] Sato Y, Sato R, Shirase K. Influence of motion error of feed drive systems onto machined surface generated by ball end mill. J Adv Mech Des Syst Manuf 2014;8(4):1–10.
[8] Nishio K, Sato R, Shirase K. Influence of motion error of feed drive systems on machined surface. J Adv Mech Des Syst Manuf 2012;6(6):781–91.
[9] Buj-Corral I, Vivancos-Calvet J, Dominguez-Fernandez A. Surface topography in ball-end milling processes as a function of feed per tooth and radial depth of cut. Int J Mach Tools Manuf 2012;53:151–9.
[10] Zheng CM, Kang YH. Mathematical modeling of chip thickness in micro-end-milling: a fourier modeling. Appl Math Model 2013;37:4208–23.
[11] Ozturk E, Taner TL, Budak E. Investigation of lead and tilt angle effects in 5-axis ball-end milling processes. Int J Mach Tools Manuf 2009;49:1053–62.
[12] Ehsan LSK, Enes YI, Ismail L. Analysis of tool orientation for 5-axis ball-end milling of flexible parts. CIRP Ann.- Manuf Tech 2015;64:97–100.
[13] Xin GL, Zhen QY. An accuracy algorithm for chip thickness modeling in 5-axis ball-end finishes milling. Comput Aided Des 2011;43:971–8.
[14] Sun Y, Ren F, Guo D, Jia Z. Estimation and experimental validation of cutting forces in ball-end milling of sculptured surfaces. Int J Mach Tools Manuf 2009;49:1238–44.
[15] Zerun Z, Rong Y, Fangyu P, Xianyin D, Lin Z, Kang S, Chaoyong G. Parametric chip thickness model based cutting forces estimation considering cutter runout of five-axis general end milling. Int J Mach Tools Manuf 2016;101:35–51.
[16] Erdim H, Lazoglu I, Ozturk B. Feedrate scheduling strategies for free-form surfaces. Int J Mach Tools Manuf 2006;46:747–57.
[17] Gong X, Yung FH. Cutter-workpiece engagement determination for general milling using triangle mesh modeling. J Comput Des Eng 2016;3(2):151–60.
[18] Ozturk E, Budak E. Modeling of 5-axis milling processes. Mach Sci Tech 2009;11:287–311.
[19] Erdim H, Sullivan A. Cutter workpiece engagement calculations for five-axis milling using composite adaptively sampled distance fields. Procedia CIRP 2013;8:438–43.
[20] Sun Y, Ren F, Guo D, Jia Z. Estimation and experimental validation of cutting forces in ball end milling of sculptured surfaces. Int J Mach Tools Manuf 2009;49:1238–44.
[21] Yucesan G, Altıntaş Y. Prediction of ball end milling forces. J Eng Ind 1996;118(1):95–103.
[22] Ko JH, Cho DW. 3D ball-end milling force model using instantaneous cutting force coefficients. J Manuf Sci Eng 2005;127(1):1–12.
[23] Altıntas Y, Lee P. Mechanics and dynamics of ball end milling. J Manuf Sci Eng 1998;120(4):684–92.
[24] Guo D, Ren F, Sun Y. An approach to modeling cutting forces in five-axis ball-end milling of curved geometries based on tool motion analysis. J Manuf Sci Eng 2010;132:1–8.